Experimental Fluid Dynamics

MAE 4273

Fall 2019

Drag Reduction Effects in Krill Aggregations

Krill Krew '19

School of Mechanical and Aerospace Engineering

Oklahoma State University

12/11/2019

Project team:

First Name	Last Name	E-mail
Trevor	Deen	trevor.deen@okstate.edu
Truc	Ngo	tructn@okstate.edu
Corey	Todd	corey.b.todd@okstate.edu
Lucas	Utley	lucas.utley@okstate.edu

AUTHORS & AUTHOR CONTRIBUTIONS

Last name	Contributions
Deen	● Wrote Physical Model Design ● Wrote Materials ● Wrote Facilities and Equipment ● Created tables 3, 4, 5, & 6 ● Final Format ● Listened to proofreading of final report
Ngo	● Wrote last section of results ● Wrote part of Conclusion ● Inserted figures into document with respective labels ● Prepared Table 1
Todd	● Wrote Experimental Protocols ● Explained Configurations in Experimental Arrangements ● Wrote Appendix and its accompanying equations ● Proofread whole report
Utley	● Wrote calculated quantities section ● Wrote abstract, introduction, and results sections ● Figure and Table captions ● Prepared data plots ● Proofread whole report

NOMENCLATURE

Symbol	Short definition	SI units
D	Drag force within fluid flow	N
C_d	Drag coefficient	(non-dimensional)
ρ	Fluid density, for this study water = 999kg/m^3 is used	kg/m^3
U	Fluid velocity	m/s
A	Frontal area with respect to flow direction	m^2
Re	Reynolds number, ratio of inertial to viscous fluid forces	(non-dimensional)
Q	Volumetric flow rate of the water tunnel (flume)	m^3/s

ABSTRACT

Antarctic krill (Euphausia superba) play a vital role in the ecosystems and food webs of southern oceans, supporting feeding habits of many species including the endangered blue whale. While krill are small organisms individually, they move and feed in huge aggregations, despite these aggregations increasing their risk of predation. This study will focus on the potential drag reduction benefits of krill aggregations to determine what percentage of drag is reduced by krill swimming in groups. To replicate the downward jet produced by swimming krill, a rigid geometry was designed for a krill test analog, enlarged in size for manufacturing purposes, and various arrangements of these analogs experienced a water flow of 3.2cm/s in a water tunnel to maintain dynamic similitude with actual smaller krill. A flexing member with strain gauges affixed measured the drag deflection of tested krill arrangements to determine if consecutive krill impact drag experienced for the overall assembly. Strain gauge voltage was measured and calibrated for drag force that ranged from 0 to 35g force for the fixed flow velocity. Results indicate that there appears to be a trend in drag reduction benefits for krill that swim linearly behind one another. The distance and depth from one krill to another has drag values up to 1.52g force, and a drag difference of 38% or greater of krill in-line versus side by side. The aggregation has been hypothesized to correspond to less swimming energy needed, and the results found in this study do support such research, but little further correlations exist from this study. Krill swim together in enormous groups, and one such reason is that the resulting wake from their swimming motion appears to correlate to less overall energy needed (less drag exists) to swim and maneuver.

1. INTRODUCTION

Antarctic krill (*Euphausia superba*) are one of the most abundant lifeforms in the ocean, making up an estimated mass of 500 million tons and trillions of individual organisms [1]. They are necessary for converting the phytoplankton on the ocean's surface into animal tissue that is consumed by larger predators including the endangered blue whale (*Balaenoptera musculus*). Krill swim in enormous schools, or aggregations, with densities within an aggregation of 20,000 to 30,000 krill per cubic meter of water [2]. Such dense groupings increase their susceptibility to predation, yet they maintain such behavior. A photo of captured swimming krill is shown in Figure 1. The spatial positioning of krill has been observed to maintain certain configurations relative to individual organisms as seen in Figure 2.

It has been studied that krill tend to swim in the induced jet from their frontal neighbor which is conducive to communication and coordination as a result of hydrodynamic signals from the neighbor's swimming jet [5]. Murphy et al studied the krill spatial positioning as a result of biological benefits such as communication and overhead sunlight availability but did not examine physical aspects such as turbulence, vorticity, or drag. Catton et al. examined flow fields resulting from krill grouping and were able to quantify ranges of krill swimming speeds and distances for various arrangements [6]. While these parameters were observed and quantified, measurements of drag force from one krill to another were not examined. Therefore, it is hypothesized in this study that krill aggregations induce a drag reduction benefit during swimming to mitigate the energy necessary for maneuvering and traveling. If true, aggregations would allow more distance to be traveled each day to promote better feeding opportunities and even avoid predation to a greater extent. These benefits may also be applicable to other species that tend to congregate in similar groups.

Objectives of this study:

1. Examine individual and pairs of a krill-like objects to understand the drag effects when swimming near surrounding neighbors.
2. Quantify drag measurements for different arrangements of krill analogs that vary nearest-neighbor elevation (NNE) to one another.
    a. By understanding the movement and reasoning behind spatial positioning as a result of swimming, the overall krill aggregation movement may be better understood and predicted as it relates to feeding habits of its predators.

2. EXPERIMENTAL ARRANGEMENTS

Physical model design:

The purpose of the 3D printed krill design was to provide a testing model that simulated the Antarctic krill swimming mechanism and body characteristics as closely as possible. In the wild, Antarctic krill average in length at about 4 cm, and have 5 pairs of legs. They are not naturally buoyant; they stay afloat by swimming in pulses segmented by rest intervals. During these swimming pulses, the krill paddle water in a downward jet focused at an angle of about 43 degrees below the horizontal, achieving an average speed of about 8 cm/s.

The goal was to match these behavioral and physical characteristics as closely as possible; however, due to the manufacturing constraints associated with 3D printing at that scale, the length of the krill models was increased to 10 cm, utilizing matching Reynolds numbers of 3200 and dynamic similitude to scale the velocity to 3.2 cm/s (equations A1, A2, A3, A4). 3D printing limitations also dictated that the 5 pairs of legs be omitted; however, the legs add minimal frontal area to the models and therefore their effect on drag is negligible. Additionally, preliminary drag calculations were performed so that they could be compared to the results at the end of the experiment. Assuming water as the fluid of interest, a frontal area of 2958 mm^2 and a drag coefficient of 2.3, the drag for a single krill was estimated to be 3.5 mN (Equation 2). To obtain the downward jet featured by swimming krill, an

internal flow section was included to divert a portion of the incoming flow downwards at that 43 degree angle. Figure 3 depicts the final krill model.

This experiment sought to inspect nine krill configurations. Configuration 1 consisted of only a single rod secured to the center of the harness as a benchmark. Configuration 2 takes Configuration 1 and adds a krill to the end of the rod. The results of the second can be compared to the first to ensure the krill models do, in fact, produce a non-negligible drag compared to the supporting rod. Configuration 3 examines a pair of krill aligned "shoulder-to-shoulder" at 5 inches measured center-to-center and suspended at an equal depth of 1 inch below the water surface. This arrangement provides a sanity check and shows that the system operates as expected, returning a much larger measured drag force in comparison to a single krill or rod alone.

Configurations 4 through 9 all consist of a pair secured in-line. The 4^{th}, 5^{th}, and 6^{th} arrangements separate the models at 1.46 Krill Body Lengths from each other, measured nose-to-nose, equidistant from the center of the mounting plate. Configurations 7, 8, and 9 feature identical characteristics, but separate the models by 1.73 Krill Body Lengths. These body lengths correspond closely to the body lengths studied by Catton et al., so that data may be compared.

In all 6 of the in-line configurations the leading krill is fastened at the same depth while the trailing krill is varied in distance from the leading krill, as well as depth relative to the leading krill. The angle between the trailing krill relative to the leading krill and the horizontal is denoted as the NNE angle, measured in degrees from the horizontal. Configurations 4, 5, and 6 inspect NNE angles of 0, 24, and 35, while configurations 7, 8, and 9 inspect NNE angles of 0, 22, and 32, respectively. As the mounting plate was constructed with mounting slots at ½ inch intervals, the trailing krill depth was determined using NNE and horizontal distance between the pair of krill. Table 1 displays the test matrix of this investigation and Figure 4 visually presents a template of the inline configurations.

Materials:

The tested 3D-printed krill models are 10 cm in length and composed of PLA plastic. The outer and inner surfaces are smooth in texture; a small section called the Dorsal Mounting Point (DMP) protrudes on the top of the inlet side and houses a 6-32" threaded mounting point. The krill models are secured to the bottom plate of the krill harness via 6-32" stainless steel all-thread rods and nylon-lined locknuts. As the models are dragged through the water, the water enters the inlet and is directed downward at an angle of 42 degrees.

To test the effect different krill configurations have on drag, the group manufactured a device dubbed the "Krill Harness." Depicted in Figure 5, the Krill harness consists of 2 strain gauges, 2 L-brackets (top and bottom), a flex plate, and a bottom plate. The L-brackets are pre-purchased stainless-steel brackets pre-drilled with ¼" holes; they serve as mounting points between the flume and flex plate, and flex plate and bottom plate, respectively. The 2 strain gauges are attached to both sides of the flex plate, a 12"x1.5"x .06" aluminum member that elastically deforms in response to drag force to produce a deflection reading from the strain gauges. The bottom plate is a 20"x1.5"x .06" aluminum member that acts as a mounting point for the krill models. The entire assembly is held together via 4x M6 stainless-steel nuts, 4x bolts, and 4x lock washers.

Facilities and Equipment:

The top plate of the krill harness was mounted to a section of extruded aluminum and secured to the top of the Endeavor Flume (GUNT GmbH, Hamburg, GER). The krill models were suspended from the bottom plate into the 8.5 m^3/hr flow of water in various configurations, depicted in Table 1. The resulting drag force caused the flex plate to bend, inducing a change in voltage across the strain gauge. The digital signal is then converted into an analog signal via a Digital Analog Converter (DAC USB-6210, Texas Instruments, Dallas, Texas, USA), processed by the signal conditioning amplifier (Model 2160, Vishay Measurements Group, Wendell, NC, USA), and recorded via a custom LabView VI (National Instruments, Austin, Texas, USA). Ultimately, the stored voltages are converted

into drag forces via a calibration curve, discussed later in the Results section. The entire process is depicted in Figure 6.

Experimental protocols:

All trials for all configurations followed identical experimental protocols. Once the configuration of interest is firmly secured to the harness, the extruded aluminum cross beam is set to rest atop the empty flume on the rails with the flex and mounting plates allowed to hang below the cross beam and the krill and rods below the plates. A stopper is secured in place on either rail via taping. These stoppers serve as reference locations to place the ends of the cross beam to ensure the entire harness returns to a position such that the krill configuration is parallel to the flow.

Because the flume in use by this investigation is incapable of holding steady a body of water without the draw gate leakage causing a measurable flow, a baseline measurement is recorded while the harness is suspended midair in the flume. Data collection is uninterrupted from this point forward and the pump is activated to generate the desired flow velocity and depth for the 12-inch width of the flume. In this investigation the pump was set to generate a volumetric flow rate of 8.5 m^3/hr, corresponding to a depth of 24.1 cm and flow velocity of 3.2 cm/s.

Once a steady depth of 24.1 cm is observed, the flow velocity is assumed steady as well. For extra assurance the flume control panel also has a display of the volumetric pump output. The presence of the operating pump produces vastly excessive noise in the observed signal, and its deactivation will have no effect upon the flow velocity and is justified by derivation in section 2 of the appendix. When the flow is assuredly steady, the pump is deactivated to remove noise and measurements are recorded for a minimum of 2 seconds after pump deactivation. At this point the data file can be saved, harness removed to prepare subsequent configurations, and the flume allowed to drain.

Calculated quantities:

Several flow parameters were calculated in this study, Reynolds number being one. Reynolds number is the ratio of inertial to viscous forces of a fluid flow and is found by Equation 1 where U is flow velocity, l is characteristic length (in this study it is the krill length horizontally, 10cm), and v is the kinematic viscosity of water = 1.05 x 10^{-6} m^2/s.

$$Re = Ul/v \tag{1}$$

Following data acquisition, drag forces were validated by calculating drag coefficient, C_d, for several configurations of krill arrangements. D is drag force obtained following strain gauge voltage conversion to calibrated drag force, ρ is density of water = 999 kg/m^3, and A is the frontal area of the krill and threaded rod suspension.

$$C_d = 2D/\rho U^2 A \tag{2}$$

4. RESULTS AND DISCUSSION

Summary:

An average of 2000 data points was calculated (2 seconds of data) at the initial zero position of krill and again after the flow reached steady state 3.2cm/s over the krill. The difference in voltage deflection was multiplied by the calibration coefficient of 0.0501 V/g to determine drag force values. 2 krill side by side produced the most drag of 4 grams, with every other configuration 36% of that or less. Clear correlations of position to drag reduction weren't determined, and large variation in calculated drag coefficient indicated issues with the data acquired and experimental setup. While less drag was observed for 2 krill in line than side by side, exact measurements of in-line variations are not witnessed.

Effects of varying number of Krill:

To reduce the data of interest, only certain regions of the raw data were examined. Figure 7 is an example of the entire raw data from Configuration 3 of krill side by side. Several regions of interest are labeled to indicate the influence of the water tunnel pump on noise impacting the strain gauge signal. The sections boxed in red in Figure 8 were used to further calculate an average. These two regions are condensed into Figure 9. Only the initial zero region was averaged as well as the region immediately after shutting off the pump, several minutes in as shown in the green regions in Figure 10. The green areas represent 2 second intervals that were averaged at the initial and final deflection position. The difference between the initial average and final average was calculated as the voltage resulting from drag deflecting the flex plate. The calibration data (Figure 11) was then applied for 1V = 19.96g force to convert all voltage differences into drag force deflections. The calibration data is shown in Figure 6.1 with the trendline for each point plotted with the known weights in Figure 12.

For the 9 configurations, some average deflection differences were negative and some positive as seen in Figure 13. This is likely the result of slight initial deflection from the krill articles not positioned directly about the bottom plate's center of gravity (CG). The implications of this are discussed in the Limitations section. However, if the absolute value of the difference is taken to examine pure deflection from original position, regardless of direction, Figure 14 is generated. First, the largest deflection shown is for the configuration of 2 krill side by side. This is 33 times greater than the deflection measured for 1 krill. Any other configuration is only 36% of the drag of the two krill side by side. This aligns with what was expected for 2 krill side by side to have the greatest frontal area, and therefore, the greatest drag measured. An issue with these measurements is the drag measured of the rod alone versus the 1 krill. A greater drag was measured for the rod alone, although the krill measurement had the krill shape as well as the same exact rod. The rod-only drag should have been less than the rod and krill combination.

Effects of varying in-line krill NNE and Drag Validation:

By studying the 6 configurations of in-line krill from Figure 14, Figure 15 results. There are not any clearly identifiable trends from one body length distance to another, but the least measured drag occurs for a NNE between 22 and 24 degrees (designations 1.2 and 2.2 in the figure). This aligns with the findings of Catton et al. that observes krill swim at the greatest velocities between 0 and 30 degrees of NNE for 1.5 and 2 body lengths of separation, perhaps due to drag reduction benefits.

To validate the drag measurements obtained, the drag coefficient, C_d, was calculated using Equation 2. from the flow velocity, frontal area of the krill and rod, and drag force. These values for configurations 1, 2, 3, 4, and 7 are shown in Table 2. There is significant variance present from 0.36 for 1 krill to 5.99 for 2 krill side by side. Not only do such high drag coefficients not exist for such shapes, the drag coefficient for 1 krill is less than that of the rod which also doesn't support published data. The drag coefficient of a cylinder at a Reynolds number of 3200 should be 1 (Figure 16), but the calculated drag coefficient in this study shows 2.78 for the rod only. Configuration 4 was close however, showing a drag coefficient of 2.28 which aligns closely with the estimated drag coefficient of 2.3 determined early in the study. This fluctuation in values indicates issues with the experimental setup and flex plate strain gauge alignment.

Limitations:

Throughout this study, it was assumed that all parts of the test rig were rigid other than the flex plate. Flume flow velocity was assumed steady and constant once a specific flow depth was achieved.

The largest limitation of this study was the mechanics of the bottom plate and flex plate. As krill are spaced on the bottom plate with threaded rod, a moment is created with respect to the flex plate supporting the krill. For identical krill and threaded rod lengths spaced evenly on either side of the flex plate, the bottom plate would be horizontal, and a proper trial could be conducted. However, due to variance in the threaded rod length and spacing that couldn't always align exactly with the bottom plate center of gravity, slight tilt is induced in the bottom plate which was measured as a small initial deflection on the strain gauge.

This CG issue is complicated further because of the zeroing performed while the harness is suspended in air. Once the flume fills with water and submerges, buoyancy of the krill may cause an additional unknown deflection prior to obtaining the final flow deflection. This behavior likely caused the positive and negative variance in deflection voltage as observed in Figure 13.

Additional limitations include the inability to measure localized flow velocity. The water tunnel flow rate was measured to be $8.5 m^3/hr$ and based upon the steady-state flow depth and flume width, the flow velocity was calculated for the desired 3.2cm/s. This method didn't directly measure the flow velocity at the downstream tunnel location which should be done for a more rigorous study.

Catton et al. discussed the effect that tethered specimens do not accurately resemble flow behavior due to the tethering circulation and vorticity produced. The specimens in this study were indeed rigidly tethered, but the exact flow behavior wasn't as important as cumulative drag force.

A final limitation of the test setup included the variance in placing the krill assembly test rig into the flume each time. Variances in the spacing and angle relative the flume boundaries likely changed from configuration to configuration. A level and measuring tape would need to be used to ensure consistent placing location between trials.

Recommendations for future work:

- Improving the experimental setup
    - Less sensitive to the effects of noise (more deflection at low drag forces)
    - Better consistency in the testing rig when manipulating variables
    - Testing more than 2 models in different formations
- Velocity of the flow should be validated for the fluid
- Further studies
    - How does the spatial positioning of the nearest neighbor elevation up to 45° and up to 3 body lengths distance of krill swimming in groups affect the drag forces?
    - How does the positioning of aggregated krill swimming in groups of various shapes affect the drag forces?
        - In-line, side by side, combination of both
    - How do drag effects vary for 3 or more krill as opposed to just 2?
    - How does the drag force of the trailing krill differ from the focal krill?

5. CONCLUSIONS

- Some amount of drag reduction appears to exist for krill in-line versus side by side
    - All configurations of in-line krill produced less drag than the side by side configuration
- This experiment neither proves or disproves the amount of drag reduction that exists for trailing krill
    - Considering the small deflection quantities, this experimental setup was not ideal in accounting for such small values

6. ACKNOWLEDGEMENTS

The team would like to thank Dr. Arvind Santhanakrishnan for faculty mentorship and providing the necessary materials to build the test rig. Thank you also to Mitch Ford and Vishwa Kasoju for their advisement in the lab and instruction in utilizing strain gauges and other lab equipment.

7. REFERENCES

[1] Ross, R. M. and Quetin, L. B. (1988). Euphausia superba: a critical review of annual production. Comp. Biochem. Physiol. 90B, 499-505.

[2] Hamner, W. M., Hamner, P. P., Strand, S. W. & Gilmer, R. W. Behavior of Antarctic krill, Euphausia superba: Chemoreception, feeding, schooling, and molting. Science 220, 433–435 (1983).

[3] The Editors of Britannica. "Drag Coefficient." Encyclopedia Britannica. https://www.britannica.com/science/fluid-physics. August 5, 2011.

TABLES

Test Matrix					
Config.	Arrangement	Krill Body Length	NNE °	Trailing Krill Depth from Frontal Krill (in)	Horizontal Distance from Frontal Krill (in)
1	One Rod (No Krill)	-	-	-	-
2	One Krill	-	-	-	-
3	Two Krill Side-by-Side	-	0	-	-
4	Two Krill Inline (1.1)	1.46	0	0	5.5
5	Two Krill Inline (1.2)		24	2.25	5
6	Two Krill Inline (1.3)		35	3.125	4.5
7	Two Krill Inline (2.1)	1.73	0	0	6.5
8	Two Krill Inline (2.2)		22	2.5	6
9	Two Krill Inline (2.3)		32	3.5	5.5

Table 1: Layout of the test matrix with the varying arrangement of krill. 9 configurations were tested with configurations 4-9 varying in-line geometries based upon NNE and NND.

Configuration	**Drag Force Measured (mN)**	**Calculated Drag Coefficient**
1 (rod only)	1.52	2.78
2 (1 krill)	1.16	0.356
3 (2 side by side)	38.9	5.99
4 (2 in line)	**7.4**	**2.28**
7 (2 in line)	14.9	4.59

Table 2: Drag coefficient validation for 5 configurations and the measured drag forces for each. Great variation exists with coefficient values near 6 in the extreme case. Configuration 4 closely matches the estimated drag coefficient of 2.3.

FIGURES

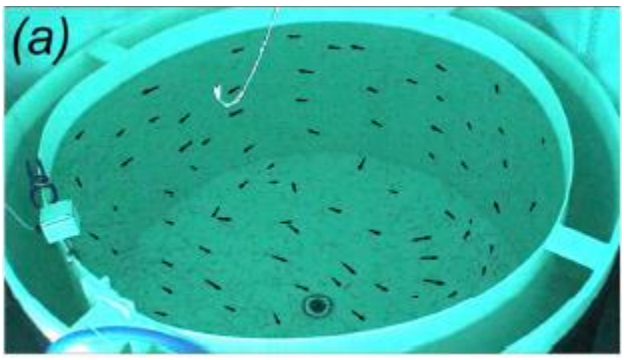

Figure 1: A captured grouping of Antarctic krill swimming together. While not in the ocean itself, this image shows the spatial distances that can exist in a krill aggregation [3].

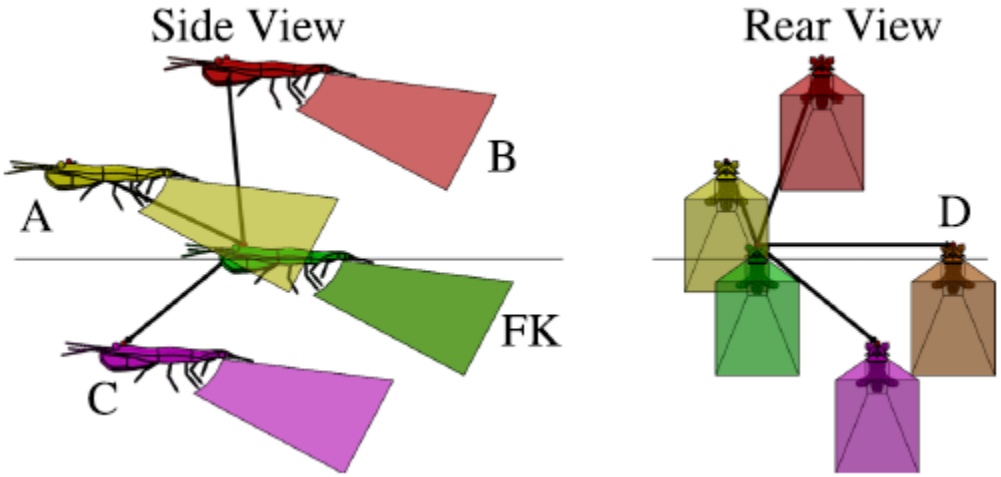

Figure 2: The shaded regions behind the krill correspond to the regions occupied by krill relative to one another with respect to the focal krill (FK). The letters denote the neighbor identification [4].

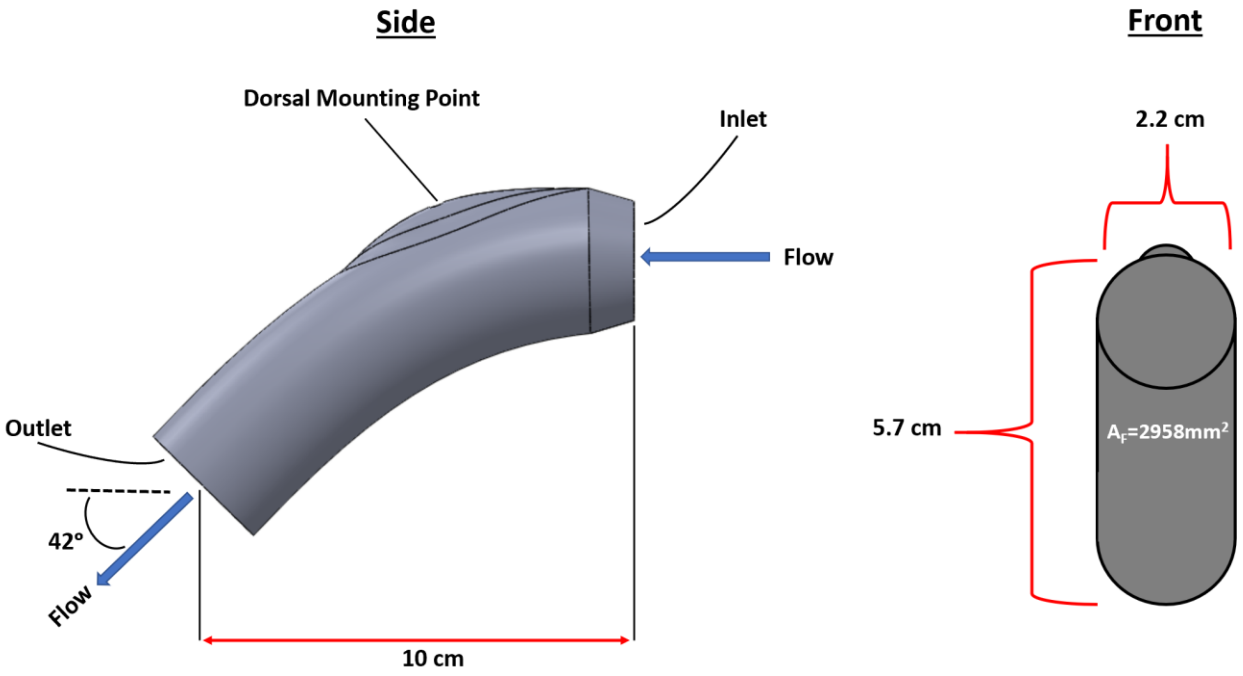

Figure 3: Side and front view of finalized krill models.

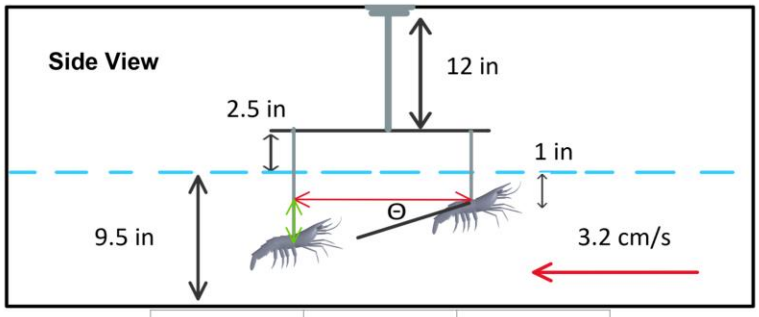

	1.73 Body Lengths	1.46 Body Lengths
Q=8.5 m^3/h	X=6.5" Y=0 Θ=0°	X=5.5" Y=0 Θ=0°
	X=6" Y=2.44" Θ=22°	X=5" Y=2.24" Θ=24°
	X=5.5" Y=3.44" Θ=32°	X=4.5" Y=3.15" Θ=35°

Figure 4: Side view of inline krill configuration. The red line is the horizontal distance between krill, the green line is the trailing krill depth, and Θ is the Nearest Neighbor Elevation Angle.

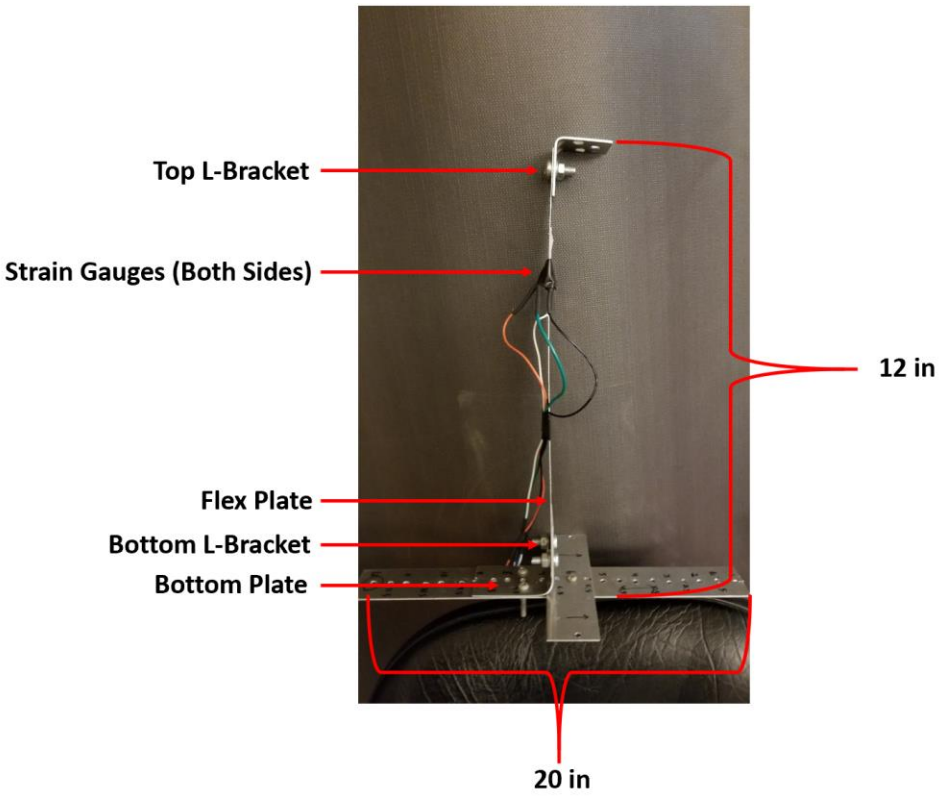

Figure 5: Test rig assembly that features the central thin aluminum flex plate (0.06in thick). The bottom plate provides the mounting points for the threaded rod and krill.

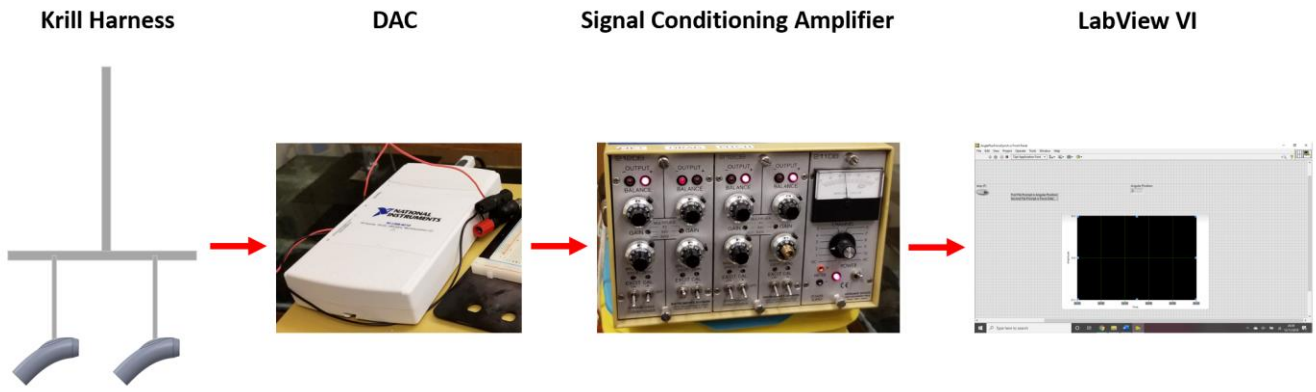

Figure 6: Experimental Facilities of krill and strain gauge to data acquisition unit to amplifier to VI for data recording.

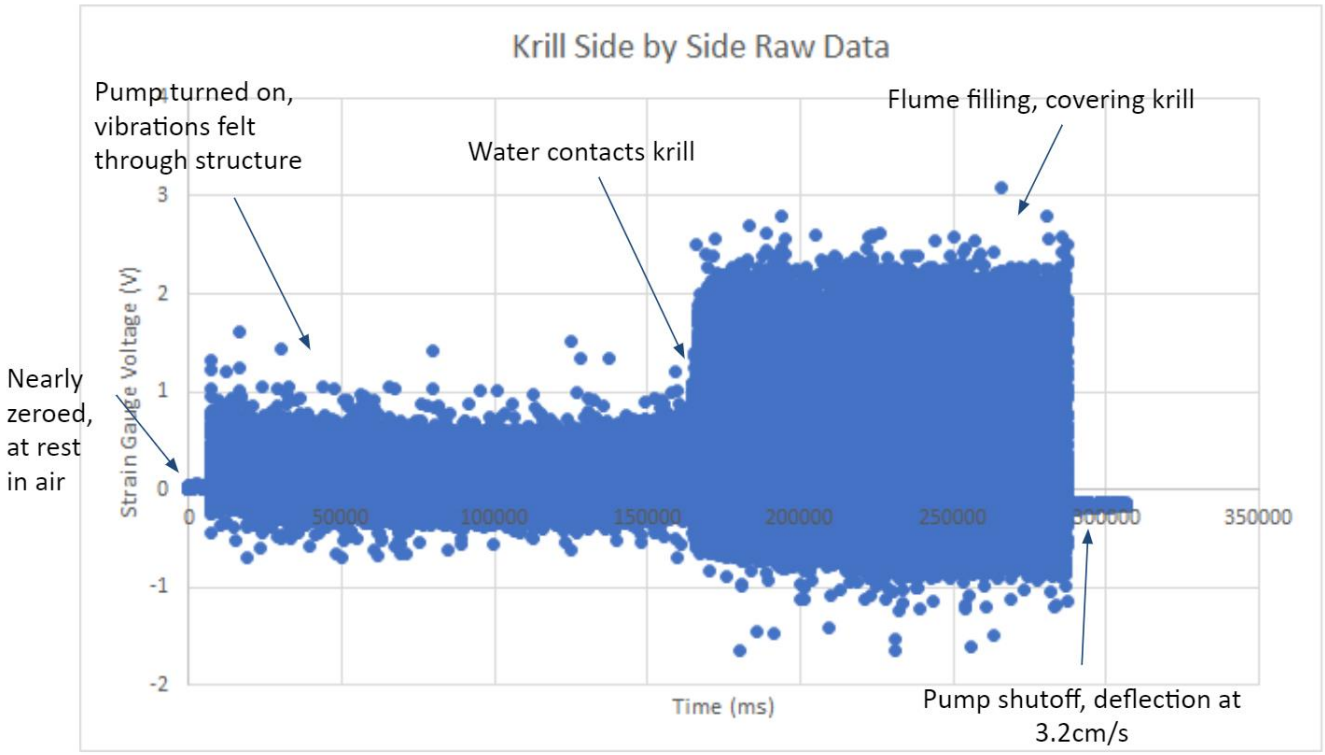

Figure 7: Cumulative data spanning 5 minutes to fill up the flume. Initial zeroed out portion is before the pump was turned on, then the signal noise is produced. The shutoff at the very end is the deflection on interest.

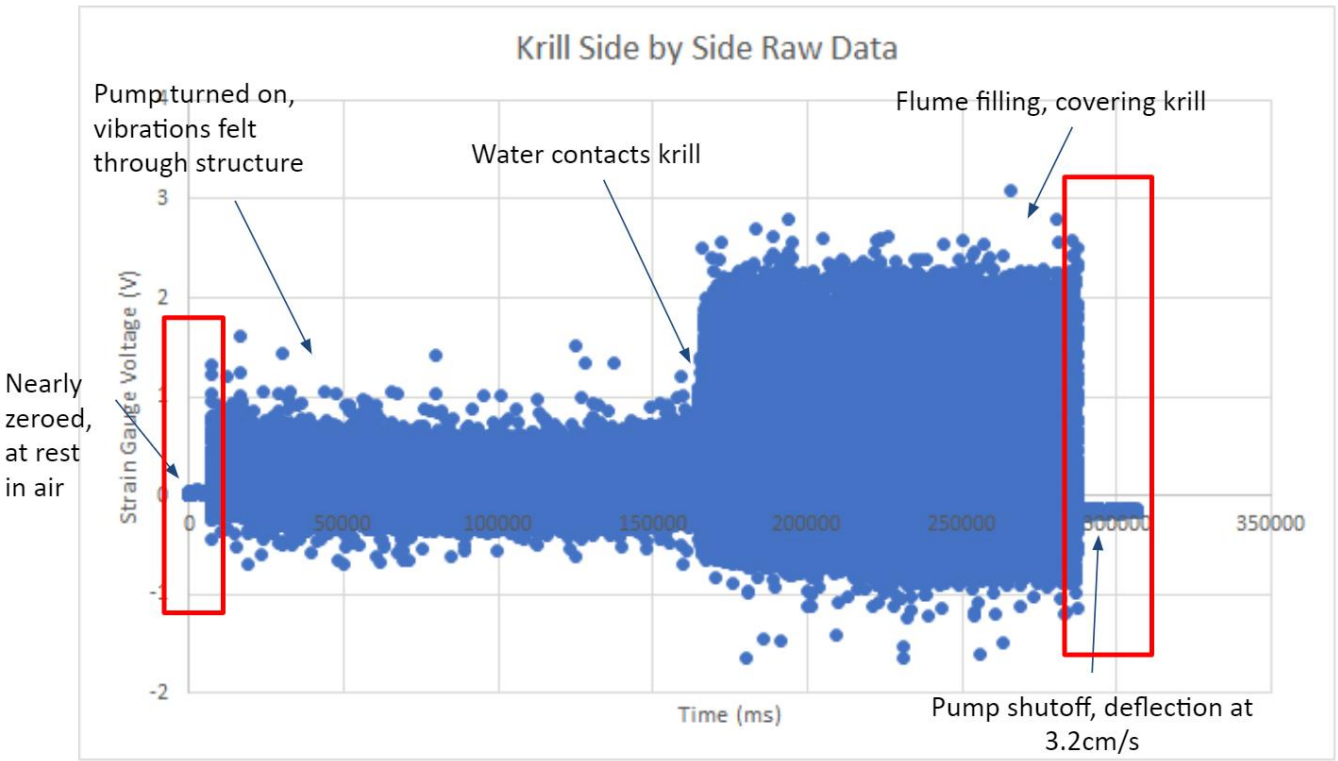

Figure 8: The red boxes indicate the data reduced to delete the in between pump noise. The only data of interest are the regions approximated within the red boxes.

Figure 9: The red boxes from Figure 8 have been expanded and plotted together in a column to zoom in on the areas of interest.

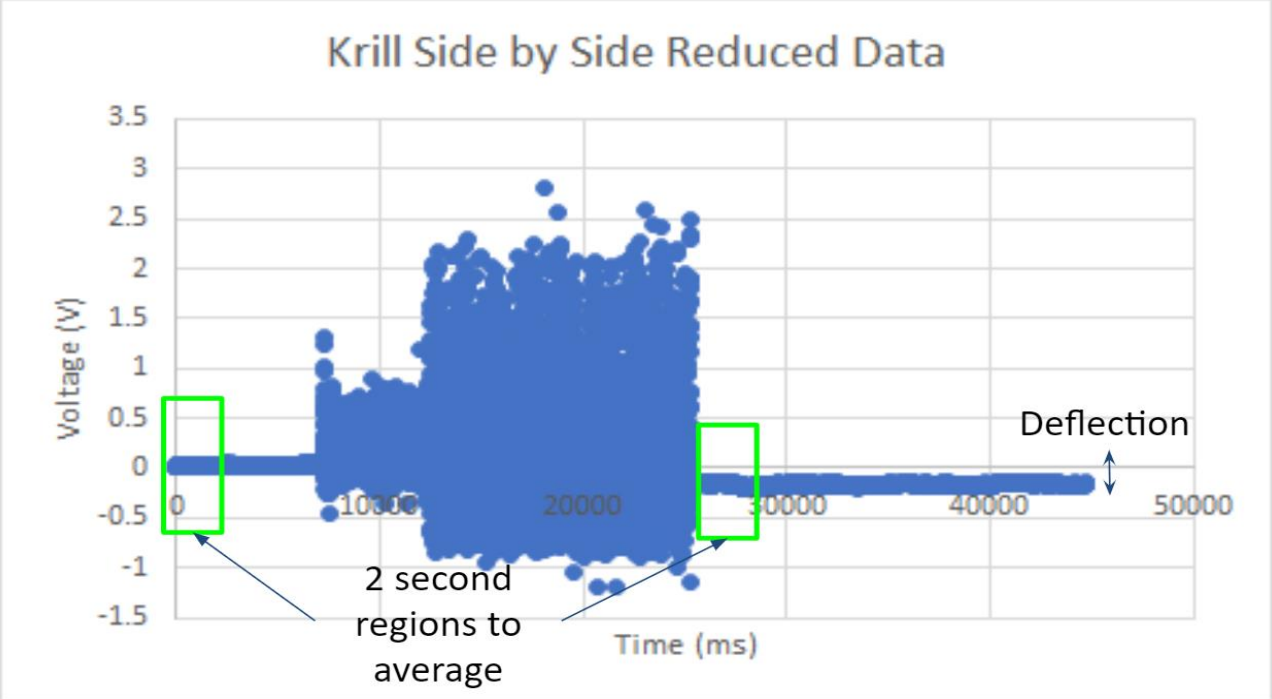

Figure 10: The green boxes are 2 seconds worth of averaged data used for comparing each configuration. 2000 data points correspond to 2 seconds of data (1000Hz sampling frequency).

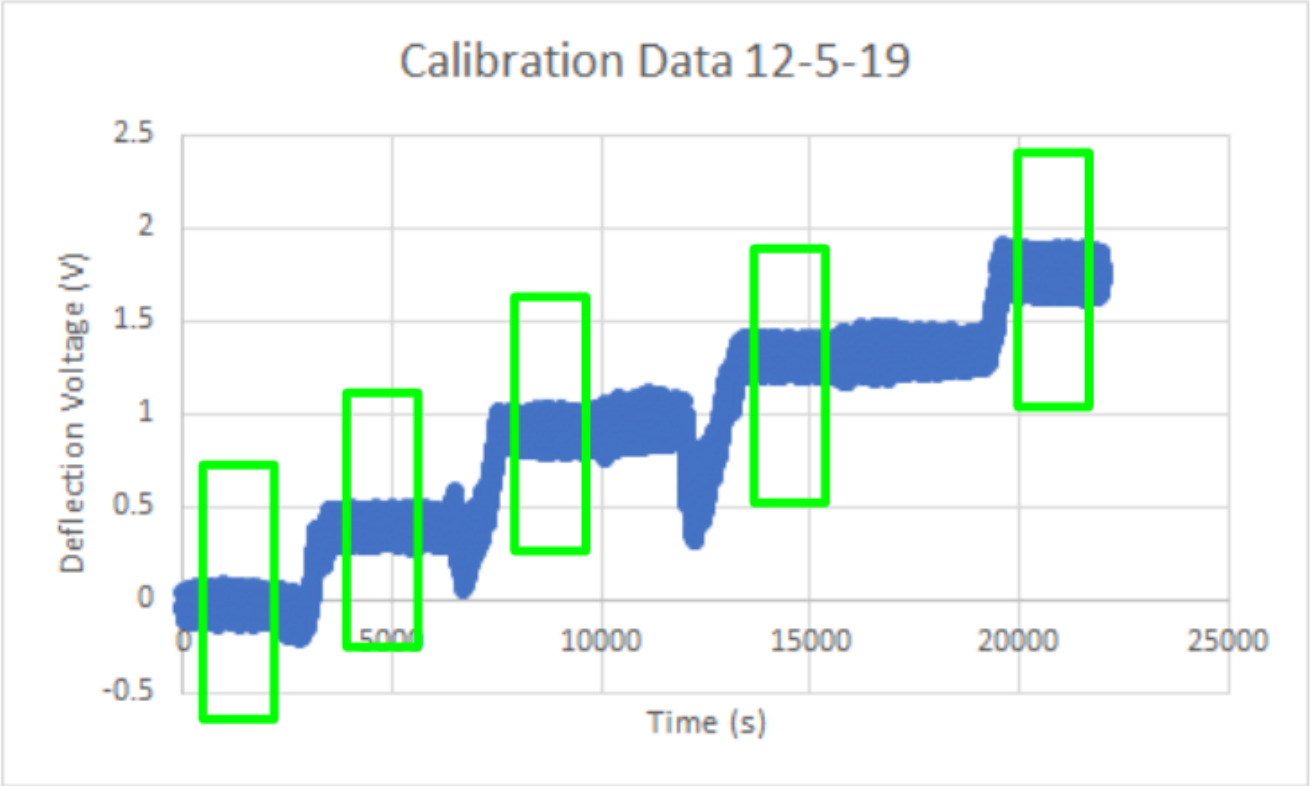

Figure 11: Calibration curve for 5 different applied weights to the bottom plate to create known forces for voltage deflections. The green boxes are representative of 2 seconds worth of acquired data at each data plateau.

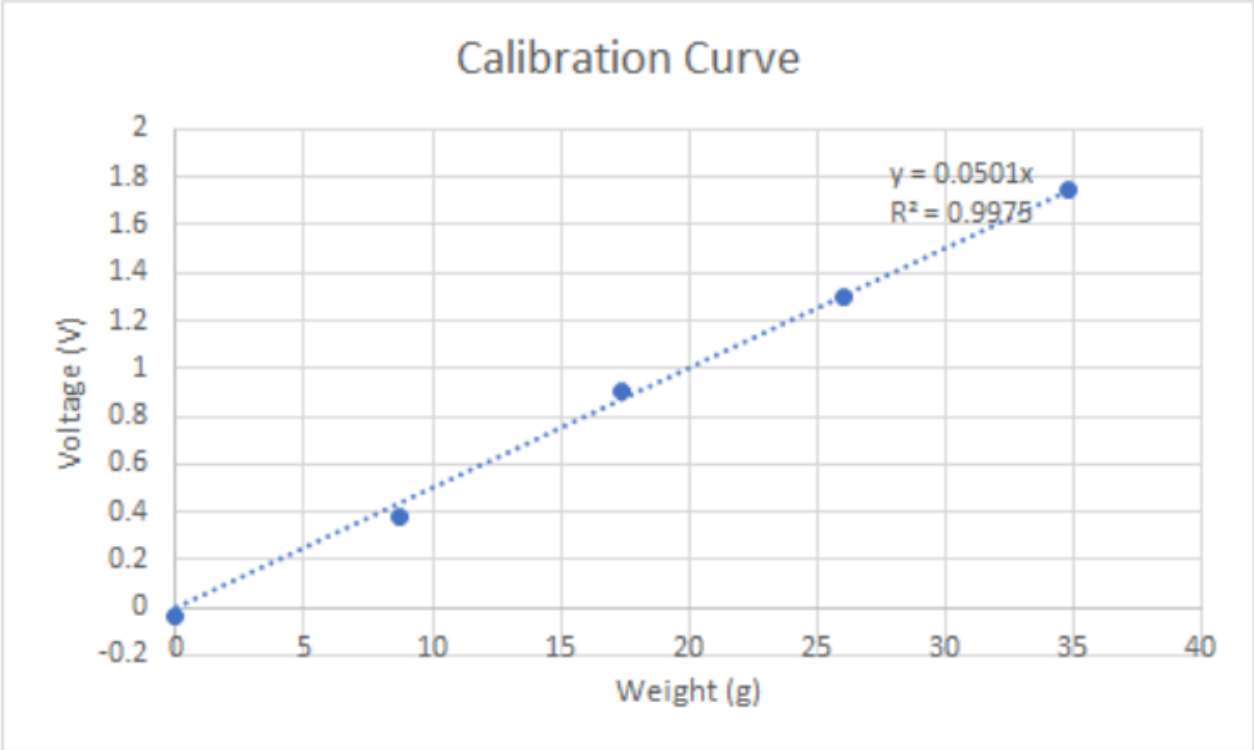

Figure 12: Plotted averages from the previous figure, graphed with the known weights of deflection. This generated the best fit trendline equation as seen on the plot.

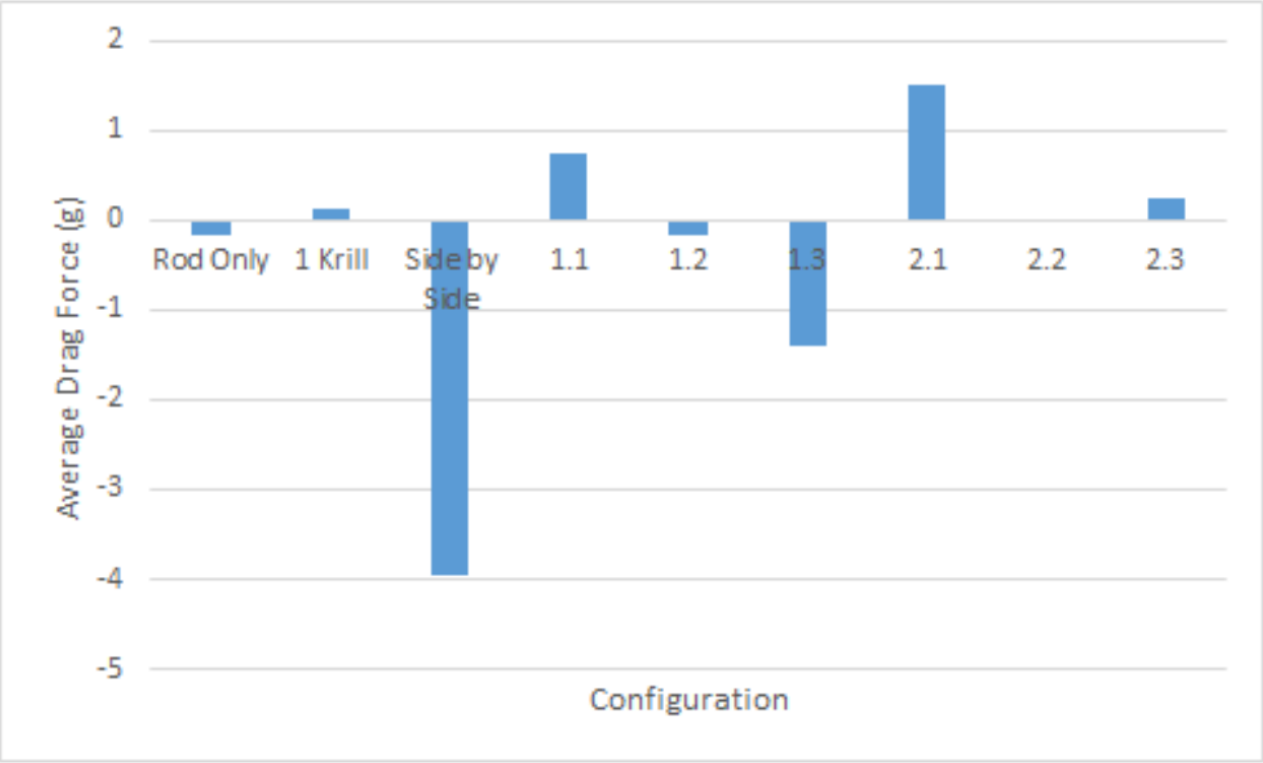

Figure 13: Averaged raw data deflection with calibration curve applied. Some values are positive and some negative, likely due to the CG issue discussed in the Limitations section.

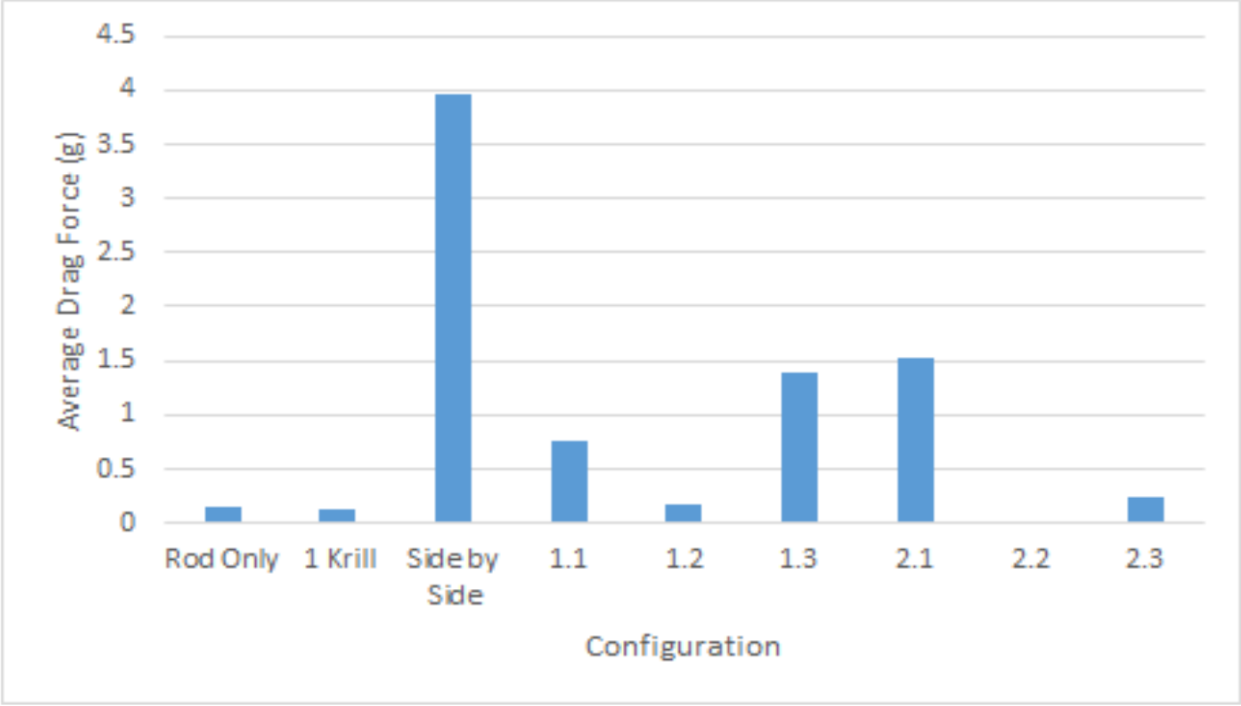

Figure 14: Absolute values taken from Figure 13 to strictly examine deflection from the taken zero point. The large deflection of side by side krill aligns with expected data that 2 krill side by side would feature greater drag. An issue with this however is apparent that 1 krill apparently has less drag than the rod by itself. This shouldn't be the case in reality.

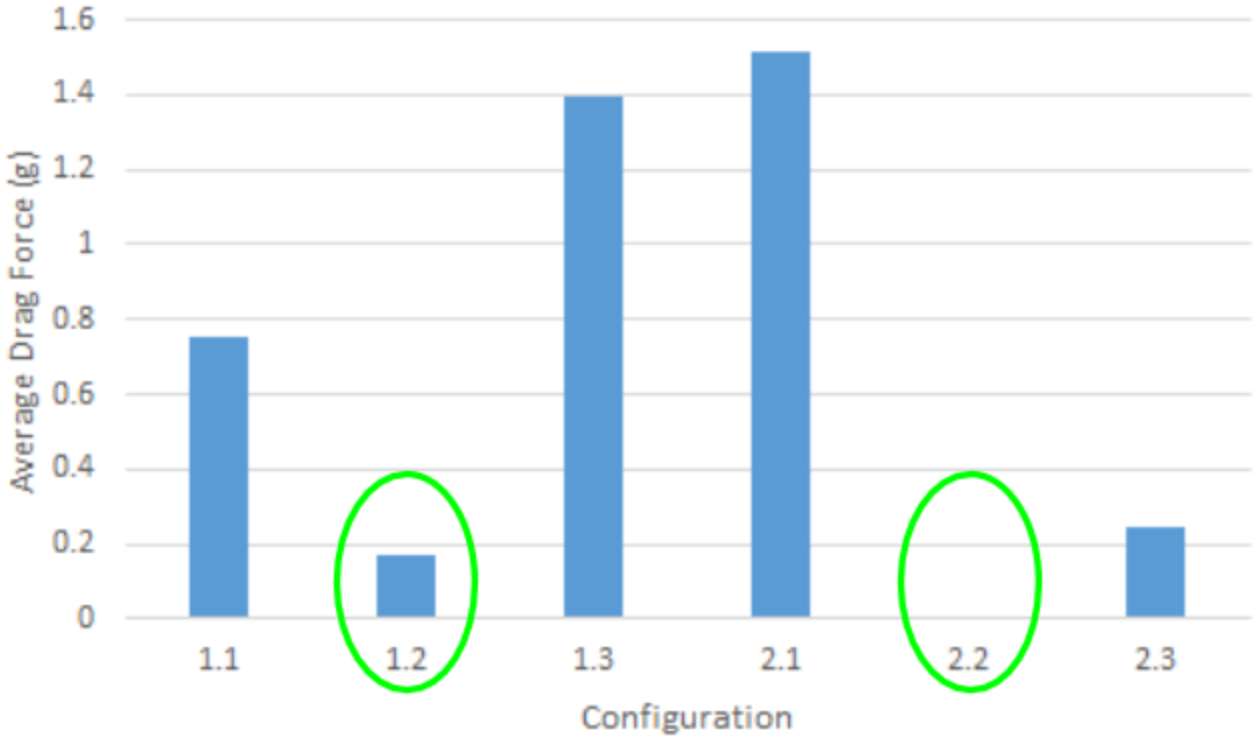

Figure 15: Here for NNE of 22 and 24 degrees, the least amount of drag was measured which supports results found from Catton et al.

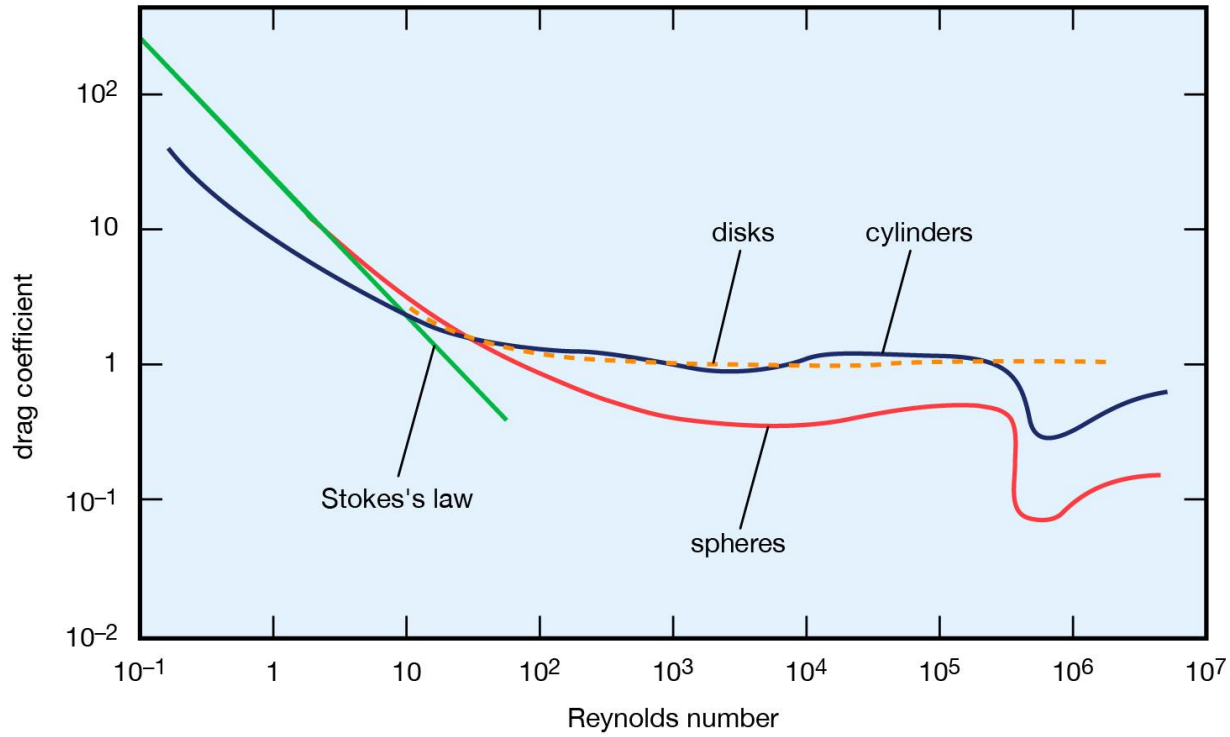

Figure 16: Drag coefficient for varying Reynolds number of several shapes [3]. For the threaded rod used to support the krill analogs in this study, C_d should be around 1 for a Reynolds number of 3200.

APPENDIX

1. Equations:

$$Re_1 = Re_2 \text{ (A1)}$$

$$\frac{\rho_1 V_1 L_1}{\mu_1} = \frac{\rho_2 V_2 L_2}{\mu_2} \text{ (A2)}$$

$$V_1 L_1 = V_2 L_2 \text{ (A4)}$$

$$V_2 = \frac{V_1 L_1}{L_2} \text{ (A4)}$$

2. Constant Flow Velocity Post Pump Shut Off:

Below is a model of the flume and the water within where:
L = Flume length, m
b = Flume length, m
h = flow depth, m
$V_1(t)$ = Velocity of surface drop after pump deactivation, m/s
$A_1(t)$ = Area of flow surface, m^2
$V_2(t)$ = Velocity of flow exiting flume, m/s
$A_2(t)$ = Cross sectional area of flow exiting flume, m/s

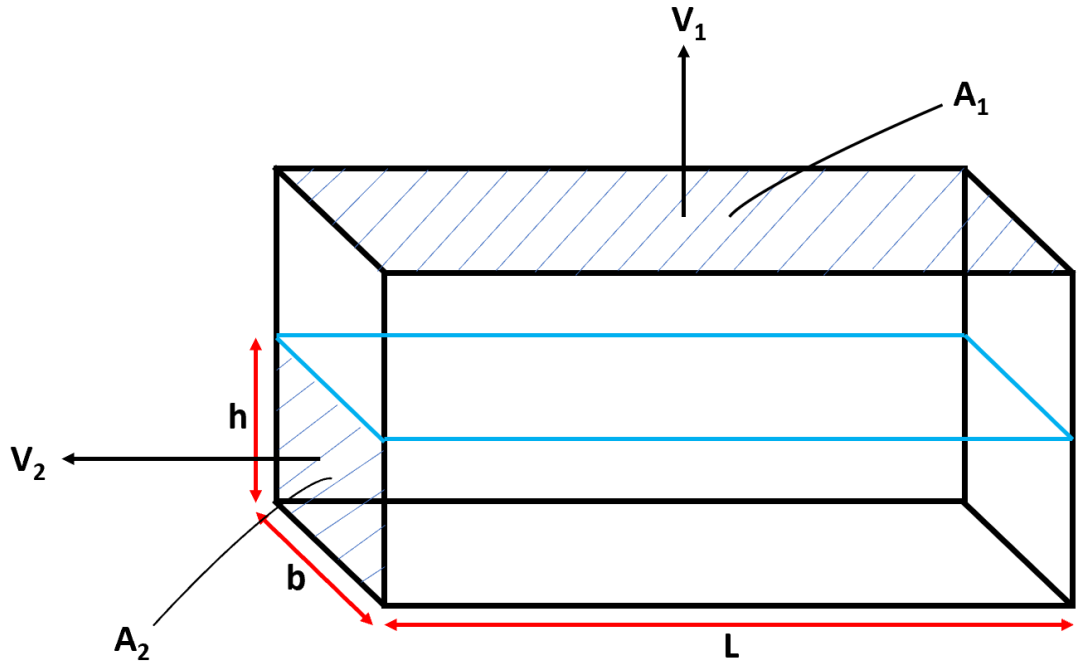

Figure A1: Control volume for flow velocity derivation.

Using a Lagrangian approach, the total initial mass of the water in the flume is equal to the sum of the masses of any water having exited the flume and any water still in the flume:

$$m_{total} = m_{in} + m_{out} = constant$$

Taking the time derivative thereof:

$$\dot{m}_{total} = \dot{m}_{in} + \dot{m}_{out} = 0$$

Rearranging yields:

$$\dot{m}_{in} = -\dot{m}_{out}$$

Expanding:

$$\rho_{in} A_{in} V_{in} = -\rho_{out} A_{out} V_{out}$$

Density is constant throughout:

$$\rho_{in} = \rho_{out}$$

The depth of the flow after pump deactivation exhibited a 1st order response of:

$$A_{in} V_{in} = -A_{out} V_{out}$$

The rate of depth change over time is V_{in}:

$$h(t) = h_0 e^{-\frac{t}{\tau}}$$

The area of inward mass flux is:

$$V_{in}(t) = -\frac{h_0}{\tau} e^{-\frac{t}{\tau}}$$

The area of outward mass flux is:

$$A_{in} = bL$$

Rearranging from above:

$$A_{out}(t) = bh(t) = bh_0 e^{-\frac{t}{\tau}}$$

Substituting from above:

$$V_{out}(t) = -\frac{V_{in}(t) A_{in}}{A_{out}(t)} = -\frac{\left[-\frac{h_0}{\tau} e^{-\frac{t}{\tau}}\right][bL]}{\left[bh_0 e^{-\frac{t}{\tau}}\right]} = \frac{L}{\tau} = constant$$

Simplifying reveals the flow velocity to be constant and proportional to flume length, L, over time constant, τ.